Periodica Polytechnica Civil Engineering

Experimental and Numerical Investigation of Cold Joint Effects on Intermediate Concrete Moment Frame Under Cyclic Loading

Amir Atashi[1], Vahidreza Kalatjari[1], Ebrahim Zamani Beydokhti[1]*

[1] Civil Engineering Department, Shahrood University of Technology, 3619995161, Shahrood, Iran
* Corresponding author, e-mail: zamani.eb@shahroodut.ac.ir

Received: 19 February 2024, Accepted: 14 October 2024, Published online: 22 October 2024

Abstract

This study investigates the seismic behavior of reinforced concrete flexural frames with a focus on the impact of cold joints (CJs). Three one-bay concrete frames, scaled to 2:3 according to ACI 318-19(22), were tested under axial and cyclic loading. The frames included a control frame without CJs, a frame with CJs, and a frame with CJs reinforced with fiber-reinforced polymer (FRP) sheets. Initially, the difference between the frame without CJs and the frame with CJs was examined, revealing a 10% reduction in cumulative energy dissipation, a 24% reduction in ductility, and an 18% reduction in lateral load capacity for the frame with CJs. Additionally, the stiffness in frames with CJs has decreased. Subsequently, the frame with CJs was reinforced with FRP sheets, leading to a 33% increase in cumulative energy dissipation and a 54% increase in lateral load capacity. However, the FRP sheets, while increasing load capacity, introduced brittleness, which reduced ductility. Crack patterns varied, with the frame without CJs showing vertical cracks near connections at 3% drifts, and the frame with CJs exhibiting tension and compression vertical cracks at 1% drifts. After validating the numerical models, two structural designs have been proposed to mitigate the negative effects of CJs in reinforced concrete structures. These designs are intended to improve seismic performance and enhance the structure's resistance to cyclic loads.

Keywords

concrete frame, cold joint, cyclic loading, seismic performance, cumulative energy dissipation, ductility

1 Introduction

The cold joint (CJ) is considered a type of weakness or defect in concrete resulting from the discontinuity of concrete pouring at different stages of construction, leading to a lack of integrity in the structural concrete. This lack of integrity can significantly affect the performance of the concrete and, ultimately, the overall behavior of the structure. The occurrence of this discontinuity at critical points in the structure (such as connections between beams and columns) may influence the seismic performance and impact the overall stability of the structure.

One of the most important components of a concrete structure is its connections. The lack of necessary capacity and ductility in the connection zone can lead to connection failures and, subsequently, the stability of the entire structure is compromised. In designs prior to 1970, the absence of transverse connection reinforcements that could provide sufficient capacity and ductility; the use of deformed rebars in connections; and their insufficient anchorage in the connection zone resulted in a decrease in the overall performance of the structures. These deficiencies could lead to the creation of plastic hinges at the beam-column connections, putting the overall stability of the structure at risk.

Other factors contributing to reduced ductility and connection weaknesses in reinforced concrete structures include differences in the timing of concrete pouring and the occurrence of CJs. Given that the construction of reinforced concrete buildings is carried out in stages, and the discontinuity of concrete pouring at specified levels is inevitable, the concrete frame is not entirely homogeneous; as a result, CJs are present in some locations.

According to the ACI 318-19(22) code [1], the placement of CJs on columns should be below the beams and above the roof slabs.

Numerous studies have been conducted in the past on the effect of CJs in beam-column connections [2–5]. Roy and

Cite this article as: Atashi, A., Kalatjari, V., Zamani Beydokhti, E. "Experimental and Numerical Investigation of Cold Joint Effects on Intermediate Concrete Moment Frame Under Cyclic Loading", Periodica Polytechnica Civil Engineering, 2024. https://doi.org/10.3311/PPci.36695

Laskar [6] studied the impact of CJs in concrete structure connections. In this study, only the beam-to-column connection was modeled and subjected to cyclic loading. The connections were modeled in two conditions, one with continuity and the other with a CJ. The results showed that in specimens with CJs, energy dissipation decreased by 24% to 49%, and ductility decreased by 22% to 36%. Furthermore, in a similar study by them [7], the initial and yield stiffness in specimens with CJs decreased by 16% to 19%. The presence of a time delay in concrete pouring is a factor in the occurrence of CJs in connections. In a study conducted by Bekem Kara [8], the time gap between two concrete pourings was examined. In this study, concrete beam specimens were used, and the results showed that as the time gap between the stages of concrete pouring increased, the compressive and flexural strength of the specimens decreased.

Qusay Ali et al. [9] investigated the critical angle of CJs in concrete. In this research, four types of concrete with compressive strengths of 10, 20, 25, and 30 megapascals were studied. CJs were formed with angles of 0 degrees (reference angle), 20, 45, 65, and 90 degrees, to understand the impact of the CJ angle on the tensile and compressive strength of concrete. The results showed that the compressive strength with CJs at angles of 0, 20, 45, and 90 degrees experienced a slight reduction, and the negative effects were not significant, with a difference of about 10% compared to specimens without CJs. However, at the 65-degree angle, the CJ significantly affected the compressive strength, resulting in a reduction of compressive strength from 5.32% to 4.48%.

Deng et al. [10] conducted experimental fatigue failure investigations on concrete members with CJs under low-stress range fatigue loading. In this research, 12 specimens were subjected to static loading, and 144 specimens were subjected to fatigue loading. The results indicate that the maximum load-bearing capacity, ductility, and fatigue life of concrete members with CJs decrease with an increase in the time gap between concrete pours and the execution of CJs.

Other studies, including those by Men et al. [11], as well as Qin et al. [12], have focused on the effects of CJs on the behavior and shear load-bearing capacity of members under cycles of dry and moist sulfate exposure.

Deng et al. [13] investigated the failure performance and fracture characteristics of concrete members with CJs using numerical simulation. Their study examined the impact of the time gap in concrete pouring on the failure performance and fracture characteristics of concrete beams with CJs through three-point bending tests and a mesoscopic model. The results showed that when the time gap between concrete pouring and the initial and final setting times exceeded certain values, the ultimate load-bearing capacity of the structure decreased by 21% and 53%, respectively.

Deng et al. [14] also focused on fatigue, crack propagation mechanisms, and measures taken in simple concrete covers with CJs in high-speed railway tunnels. Kim et al. [15] developed a new connection method using deformed and helical rebars for reinforced concrete beams with CJs. Fu et al. [16] conducted laboratory experiments to investigate the effect of the concrete pouring distance on the failure performance of concrete structures with CJs. They performed three-point bending tests on concrete members with CJs at different concrete pouring distances and examined the impact of these distances on failure performance from four aspects: crack width, fracture surface characteristics, P-CMOD curve, and dual-fracture parameters.

The results showed that with an increase in the distance of concrete pouring, crack width decreased, the expansion path converged towards the adjacent CJ, and the surface roughness and fractal dimension decreased with the extension of the distance. Feng et al. [17] and Firdaus et al. [18] also conducted investigations on composite steel-concrete connections with CJs.

Given that the concrete pouring process can sometimes be delayed for various reasons, leading to the occurrence of CJs in the beam-column connection and different sections of a concrete frame, it is essential to thoroughly investigate the impact of CJs on seismic behavior, especially the reduction in load-bearing capacity and ductility, in reinforced concrete frames. Necessary strategies to mitigate these effects, such as the use of fiber-reinforced polymer (FRP) materials in the beam-column connection region, need to be studied.

Therefore, the overall objective of this research is to examine the influence of CJs on the seismic behavior of reinforced concrete frames, including lateral load capacity, ductility, and energy absorption capacity under cyclic loading. Additionally, the study aims to assess the impact of employing FRP materials in the connection region to enhance the seismic performance of frames with CJs.

2 Properties of experimental specimens

In this study, three structural frame models were employed: Frame 1, without CJs; Frame 2, which includes CJs at connection points; and Frame 3, also with CJs but retrofitted using FRP sheets. The goal was to explore the effects of

CJs and to assess how FRP retrofitting influences the seismic performance of the structure. The properties of the three experimental specimens are presented in Table 1.

2.1 Specimens geometries

The dimensions, concrete and steel properties, as well as the magnitude of cyclic and axial loading, were the same for all three tested concrete frames. Fig. 1 provides an overview of the frame geometry, including details of the rebar and stirrup properties. The cross-section dimensions of the upper beam and lateral columns are 200 × 200 mm, while the lower beam has a cross-section of 300 × 300 mm. Additionally, Fig. 1 shows the properties of the rebars used in the beams and columns, including their type, size, and distribution. This information is crucial for a precise analysis of the structural behavior of the frames under lateral and axial loading.

The overall height of the frame is 2 m, and other properties of the frame are shown in Fig. 1. The frame scale is 2:3 and is designed based on the ACI 318-19(22) code [1]. The dimensions of the frame were selected to be realistic and demonstrate more accurate seismic behavior. Considering that the reinforced concrete placement of concrete structures is vertical, the example specimen without the CJ was cast vertically. In the CJ frame, the foundation was cast first, followed by the columns, and finally, the beams. The time interval between each concrete placement step was 7 days. In the case of a reference joint (RJ) without a CJ, concrete was poured vertically in one step. Fig. 2 shows a schematically of the used frame for reinforced concrete frames after casting concrete with a and a CJ. Fig. 3 shows a schematic of the FRP-retrofitted cold joint (RCJ) and details of the reinforcement area.

The wet lay-up method was used to reinforce the RCJ specimen with fiber. After preparing the adhesive, either rollers or standard brushes were employed, depending on the specimen's surface, to spread the coating layer uniformly. The first layer of fiber was then carefully placed and secured tightly in the connection area. A small tensile load was applied, causing the glue to seep through the

Table 1 Properties of the specimens studied in this research

Model name	Model properties
RJ	An intermediate concrete moment frame without CJs.
CJ	An intermediate concrete moment frame with CJs.
RCJ	An intermediate concrete moment frame with CJs, where the connections are strengthened with FRP sheets.

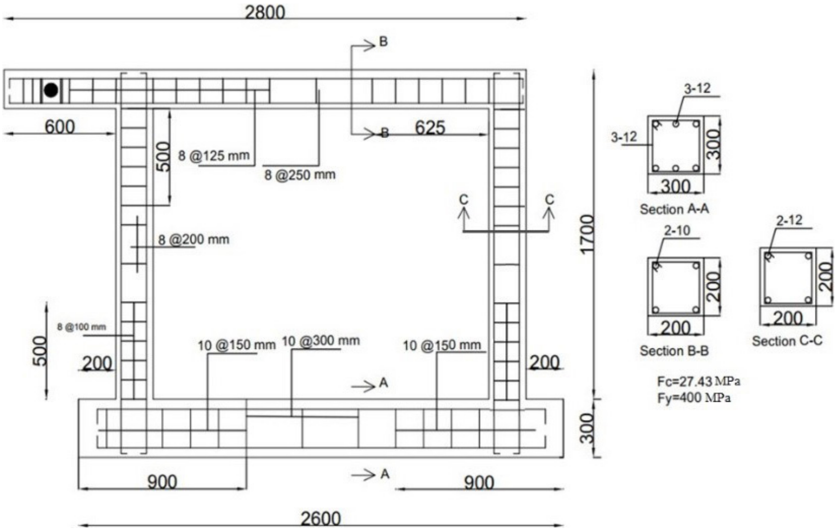

Fig. 1 Geometric dimensions and properties of the frame reinforcements

(a) (b) (c)

Fig. 2 Schematic of the mold and specimens with CJs used in this research; (a) Concrete mold; (b) RJ frame; (c) CJ frame

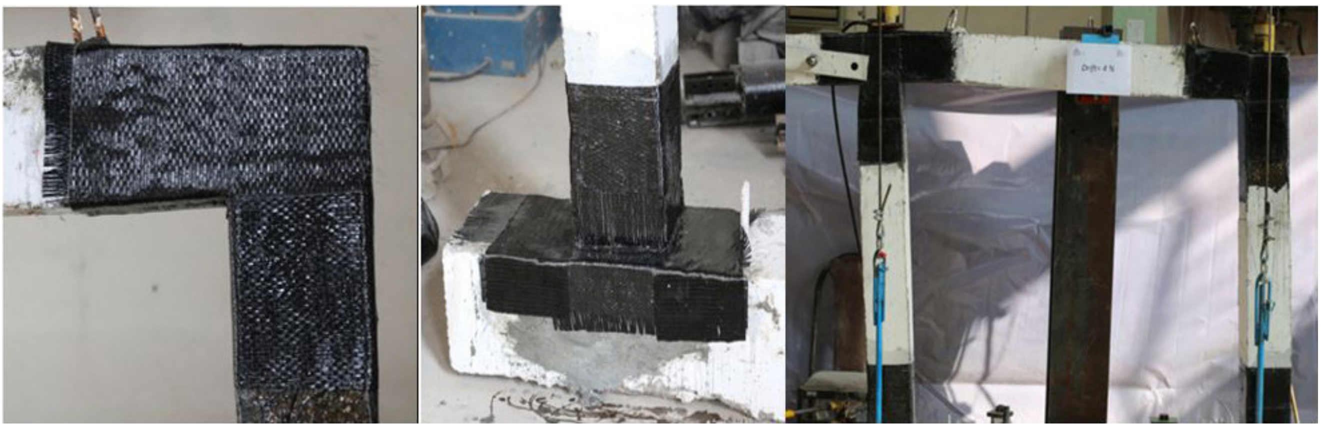

Fig. 3 Schematic of the RCJ specimen, along with details of the region retrofitted with FRP

fiber's holes. Subsequently, modest compressive stress was applied using a plastic roller on the fiber surface in one direction to avoid distortion of the composite layer, remove trapped air, and ensure a complete bond between the fiber and the specimen surface. The first layer was then covered with a connection layer adhesive, which was applied with a brush to prevent distortion. The second layer of fiber was affixed to the specimen using the same method as the first layer. After applying load with the roller, removing trapped air, and ensuring that the glue permeated the holes of the second layer of fiber, a saturated layer of adhesive was applied to complete the bonding process and create a uniform surface, particularly at the ends of the fiber and the overlapping area. Finally, to ensure proper curing and to prevent dust from contaminating the applied adhesive, a thin layer of cellophane was placed over the specimen.

In this research, a one-directional carbon fiber and epoxy resin, supplied by QUANTUM Company, were used to reinforce a CJ frame. The properties of C300 carbon fiber and EPR 3031 epoxy resin are detailed in Tables 2 and 3. The carbon fiber was provided in 100 meter rolls, and the two-component adhesive was supplied in 10 kg packs.

2.2 Material properties

Seven cubic samples were prepared to determine the compressive strength of the concrete. The cubic samples were tested at the ages of 7 days and 28 days. Table 4 presents the concrete mix design used in this research, along with

Table 2 Mechanical properties of FRP fiber

Description	Density (gr/cm^3)	Maximum length increase (%)	Elasticity modulus (GPa)	Tensile strength (MPa)	Thickness (mm)	Fiber type
One-directional high-strength carbon fiber	1.8	1.5	240	2950	0.167	C300

Table 3 Mechanical properties of the EPR-3031 glue

Descriptions	Unit
Density	1.5 (kg/l)
Minimum connection strength (during the concrete failure)	3.5 (MPa)
7 days compressive strength	95 (MPa)
Minimum tensile and flexural strength	30 (MPa)
Ultimate curing time	7 days
Implementation opportunity (initial setting)	60 min

Table 4 Concrete mix design used in the study with the average compressive strength in specimens

Compressive strength average – 28 days (MPa)	Slump (mm)	Gravel 4–20 mm (kg/m^3)	Sand 0–4 mm (kg/m^3)	Cement (kg/m^3)	Cement type	Water (L)	Water to cement ratio
27.43	61	1174	795	400	Portland type 2	160	0.4

the average compressive strength of the tested specimens. Fig. 4 illustrates a schematic of the cubic specimens and the compressive strength testing apparatus.

2.3 Loading and boundary conditions in specimens

After completing the final concrete placement and allowing a curing period of 28 days, the constructed concrete frames were connected to the solid frame of the structural laboratory and subjected to lateral and axial loading. For the lateral loading protocol, the end of the frame's console was connected to the actuator, as shown in Fig. 5. The frame was anchored to the solid floor, and movement in the out-of-plane and horizontal directions at the base of the column was restricted. Additionally, as indicated by the yellow box at the top of Fig. 5, a restraint system using two sheaves was employed to prevent lateral movement of the frame. The range, magnitude of flexural moments, and effective rotation of the columns, as well as their variations during a seismic event, were evaluated using a cyclic loading protocol. This protocol involved applying one lateral load in combination with two axial loads to simulate realistic seismic conditions.

Most experiments on the frame are performed by applying horizontal displacement cycles at the end of the element (corresponding to the story drift) in the presence of a constant axial load. For example, Kurata et al. applied horizontal displacement cycles to the free end of the columns of the box-shaped specimen [19]. Fig. 6 illustrates

Fig. 4 Compressive strength test of cubic specimens

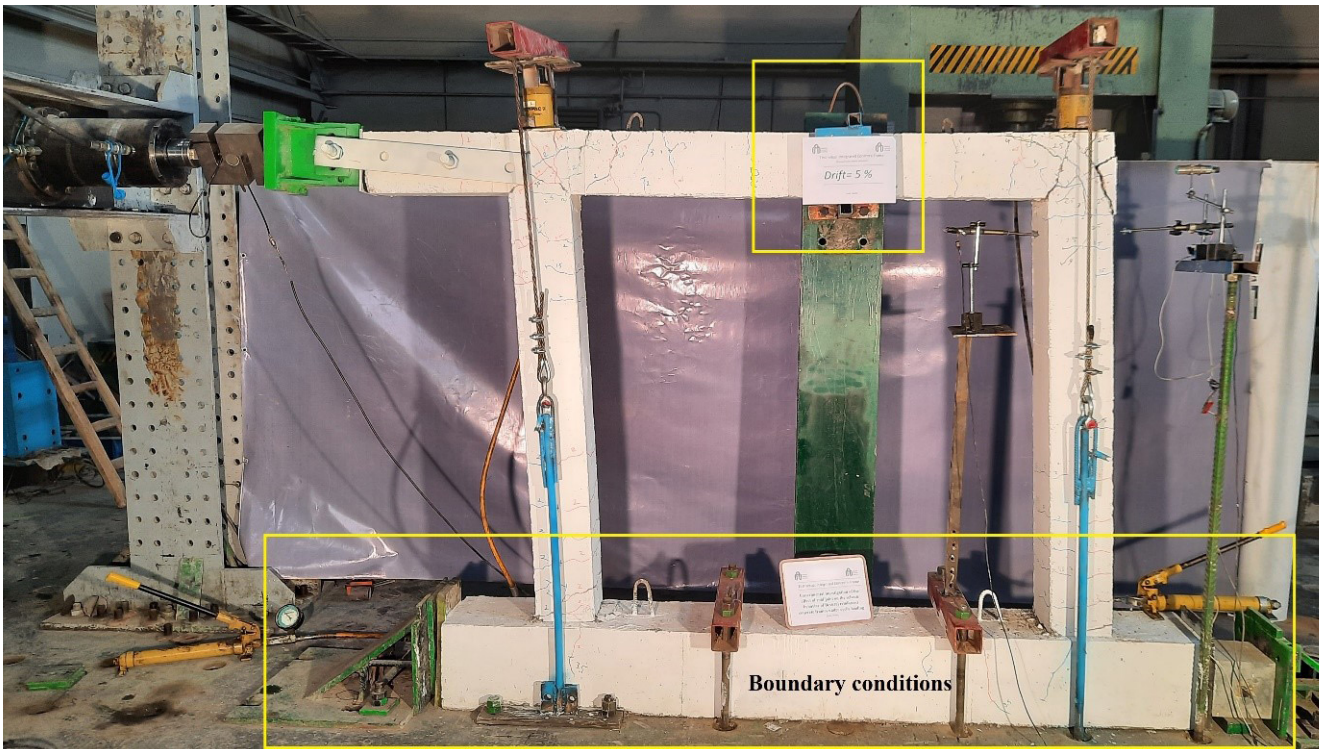

Fig. 5 Properties of the experimental specimen with lateral restraining of the frame

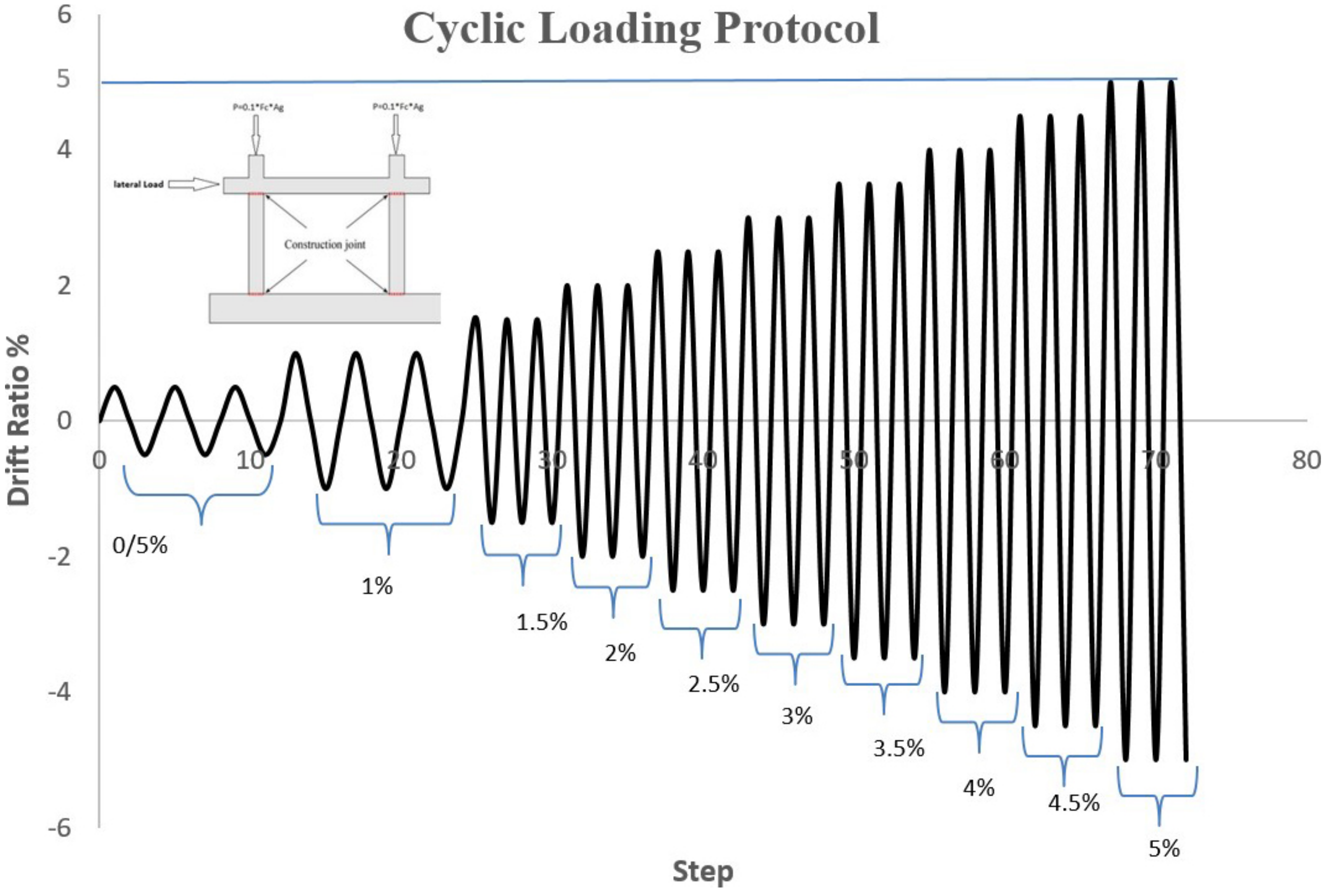

Fig. 6 Number of cycles and applied lateral displacement in the frames

the cyclic loading protocol. In this diagram, the vertical axis represents the drift percentage, while the horizontal axis shows the number of loading cycles.

According to the ACI PRC-374.2-13 [20] standard, an axial force of $P = 0.1\ F_c \times A_g$ (where A_g is the total cross-sectional area of the column and F_c is the compressive strength) was applied. The effect of axial load on each column was carefully considered. To apply lateral and axial loads to the structure, hydraulic jacks were used, as illustrated in Fig. 7.

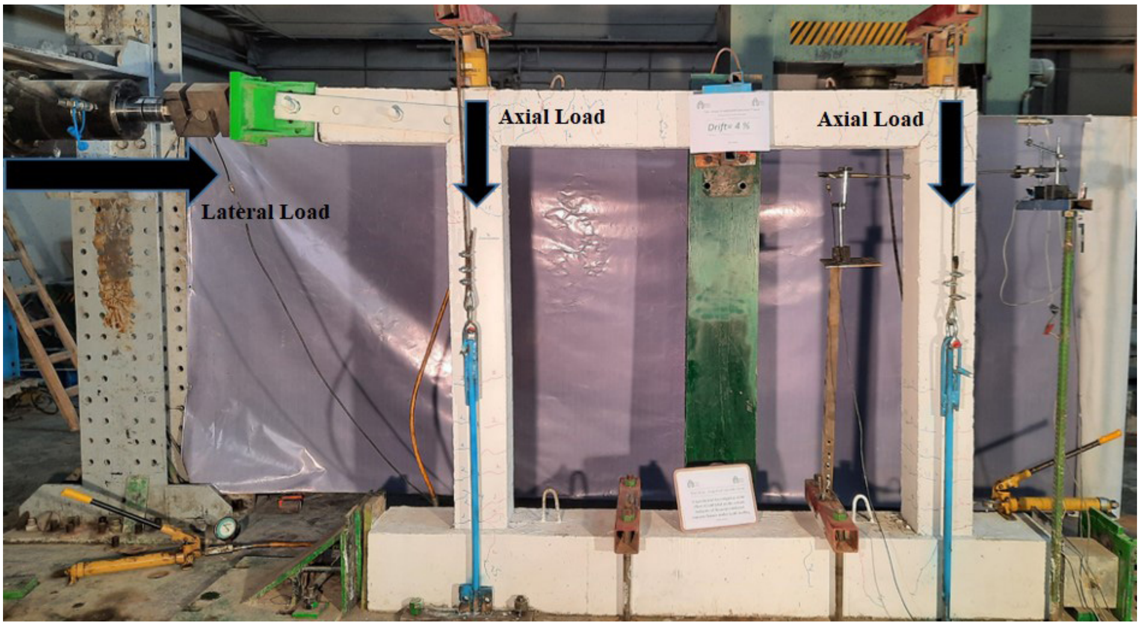

Fig. 7 Method of applying lateral and axial loads to the frame

Additionally, as shown in Fig. 8, a pipe with double the number of transverse reinforcements was used in the console to minimize the impact of demolition at the connection between the solid jack and the concrete beam. This pipe was connected to the frame in a way that did not adversely affect its stiffness. Furthermore, to precisely measure the lateral movements of the frame and the beam-to-column connection, five LVDTs were employed, as depicted in Fig. 9 These measures were implemented to ensure measurement accuracy and to analyze the structural behavior under various loading conditions.

In Fig. 9:

- LVDT 1: calculates the horizontal movement of the frame, which can be used to calculate horizontal displacement and the frame drift.
- LVDT 2: calculates the vertical movement, if any exists.
- LVDT 3 and LVDT 5: shows the displacement of both sides of the connection.
- LVDT 4: calculates the internal frame displacement.

3 Numerical models simulation in Abaqus

Section 3 involves properties of simulated models in Abaqus. RJ and CJ models were modeled and analyzed, and their results were compared to experimental results. The geometric properties of the models are shown in Fig. 1. Fig. 10 shows the numerical model of RJ and CJ frames in Abaqus software [21] for concrete modeling and rebar layout. A small area was created for modeling the CJ frame in the connection area of the column to the foundation and top beam, and concrete with poor properties was created (maximum compressive strength of 10 MPa) to simulate the CJ. Although this reduced strength in the CJ area was incorporated into the model, it did not significantly affect the overall simulation results.

Fig. 8 Using a doubled stirrup in the console connected to the concrete frame (cyclic load application area)

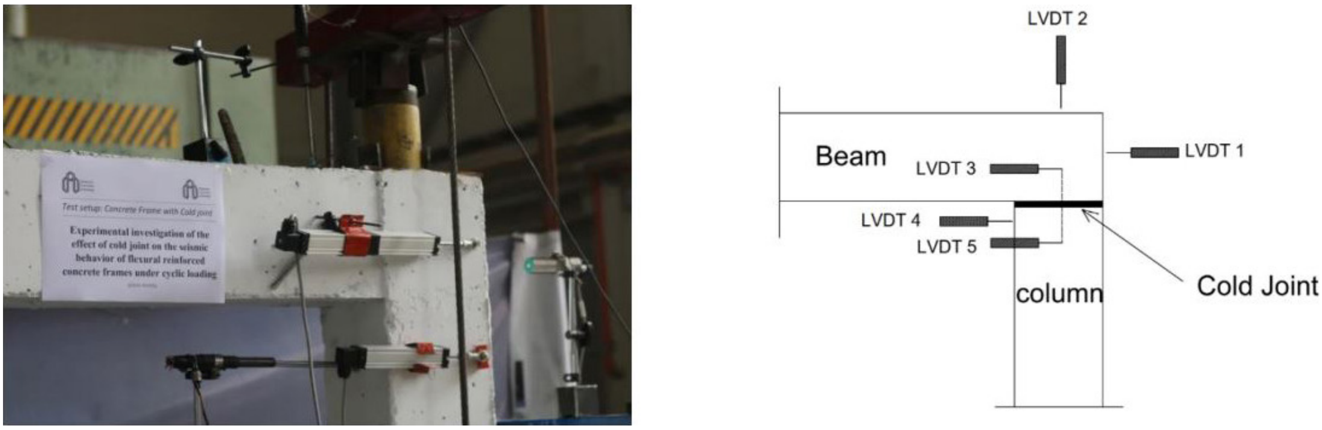

Fig. 9 Location of the LVDT in the main frame

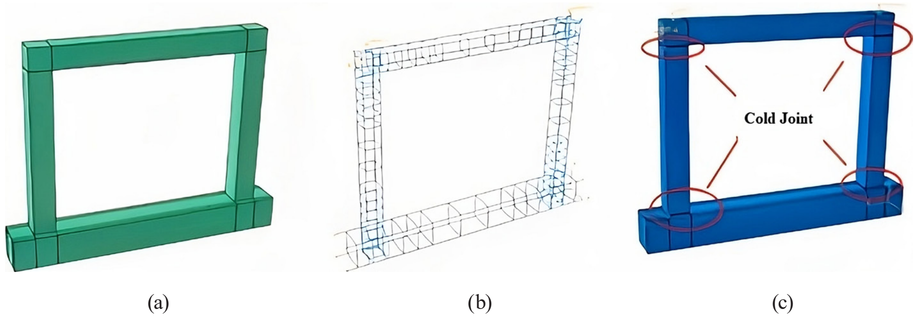

(a) (b) (c)

Fig. 10 Numerical model; (a) Geometry of the concrete section in the monolithic concrete model; (b) Geometry of rebars and stirrups; (c) Geometry of the CJ model

The compressive strength of the concrete used for modeling the concrete component is 27.34 MPa, while the yield stress of the rebars and stirrups is 400 MPa. The mechanical properties of the rebars were determined through tensile tests and imported into the software. Fig. 11 displays the stress-strain curve obtained from the tensile tests. Table 5 lists the properties of the materials used in the numerical model. Isotropic stiffening in the plastic region was employed for modeling steel. The nonlinear behavior of concrete in Abaqus was defined using the concrete damage plasticity (CDP) model, with the associated parameters shown in Table 6. Rebars and stirrups were modeled as wires using truss elements. The slippage of rebars within the concrete was modeled using the Embedded Region Constraint. Lateral loads were applied cyclically, and two 100 kN compressive loads were applied along the longitudinal axis of the columns. A pseudo-dynamic cyclic lateral load was applied to the left side of the structure. To enhance accuracy, all physical elements in the reinforced concrete, including both concrete and steel reinforcement, were modeled separately. An 8-node linear hexahedral solid element with reduced integration (C3D8R) was used for modeling concrete, and a 2-node linear beam element was used for the reinforcement. A schematic of meshing is shown in Fig. 12 [22–25].

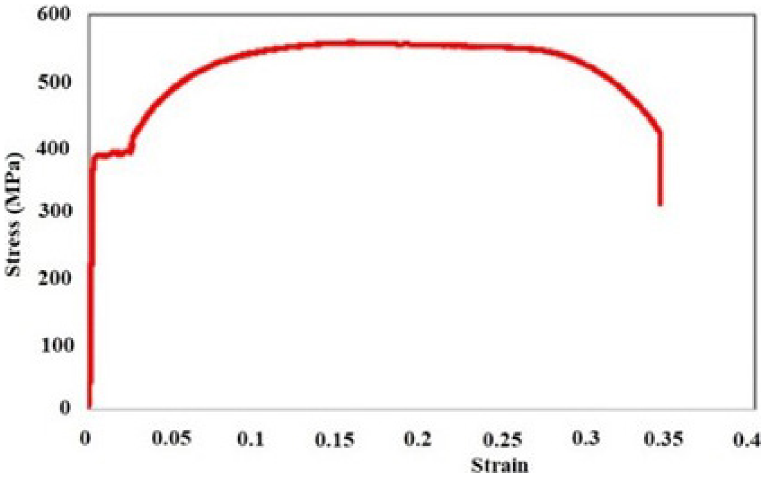

Fig. 11 Results of the tensile test for rebars

Table 5 Mechanical properties of the materials used in the numerical model

Material name	Elasticity modulus (GPa)	Poisson's coefficient	Yielding stress (MPa)	Maximum compressive strength (MPa)
Concrete	25	0.2	–	27.34
CJ concrete	15	0.2	–	10
Reinforcements	200	0.3	400	–

Table 6 CDP model parameters for simulating concrete behavior in Abaqus

Dilation angle	Eccentricity	f_{b0}/f_{c0}	K	Viscosity parameter
35	0.1	1.16	0.667	0.001

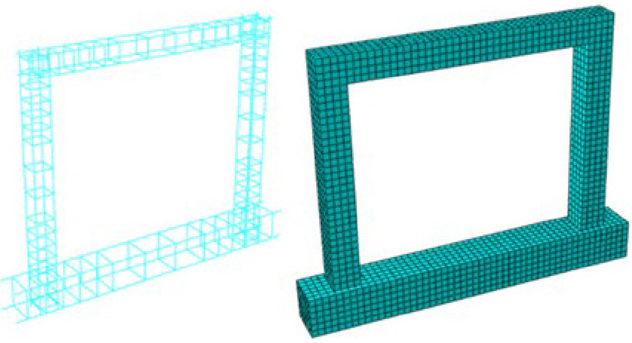

Fig. 12 Meshing the concrete part and reinforcement

4 Experimental results and discussion

Section 4 presents the results related to the laboratory samples and provides a comprehensive analysis of their characteristics. The results include an analysis of sample failure, which helps identify weaknesses and potential causes of failure under various loading conditions; an examination of hysteresis curves to understand the behavior of samples under cyclic loading and their capacity to absorb and dissipate energy; an assessment of strength degradation throughout the test and its impact on overall structural performance; an evaluation of stiffness reduction and its effects on both dynamic and static behavior of the structure; a measurement of the samples' ductility and their ability to withstand shape changes under severe loading conditions; and a calculation of dissipated energy, which aids in analyzing the structure's efficiency in absorbing and distributing energy.

4.1 Failure of the frames

The crack patterns observed in the RJ specimen, CJ specimen, and RCJ specimen at various drift levels are shown in Figs. 13 to 15, respectively. These crack patterns are critical for understanding the behavior of each specimen under lateral loading, as they provide insight into the structural integrity and failure mechanisms of the frames. By comparing the crack patterns, the effects of CJs and retrofitted joints on the structural performance can be assessed, contributing to a deeper understanding of their impact under seismic conditions.

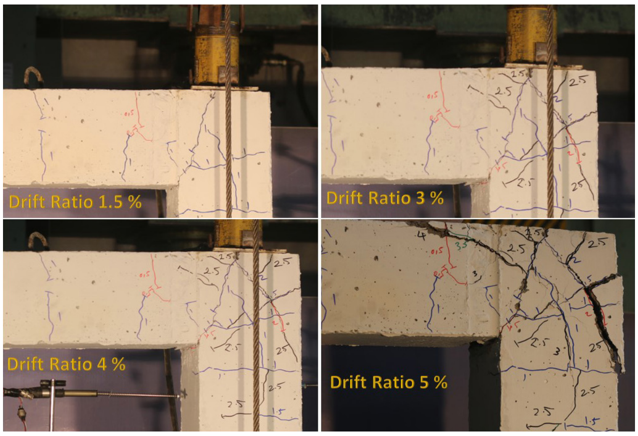

Fig. 13 The pattern of crack formation in various drifts within RJ frame

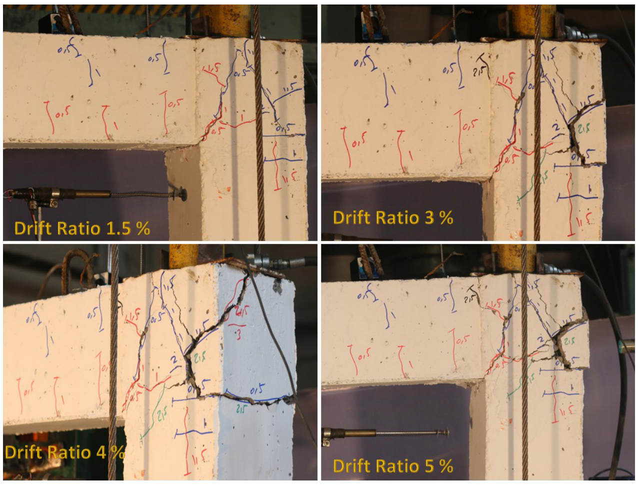

Fig. 14 The pattern of crack formation in various drifts within CJ frame

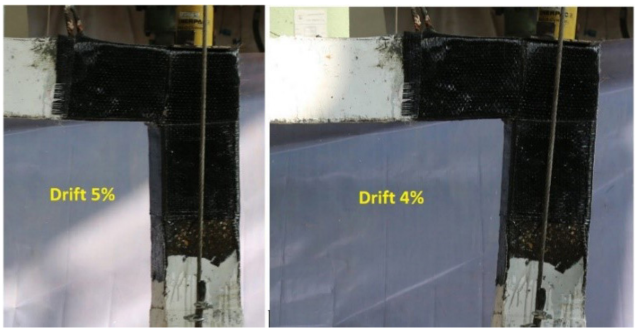

Fig. 15 Behavior of RCJ frame

Based on the conducted studies and experimental observations, the impact of CJs in reinforced concrete structures is clearly evident. As shown in Fig. 13, in Frame RJ, superficial cracks with short lengths appeared at drift levels of 1% to 2%. Due to the absence of CJs and the uniformity of the concrete, these cracks were relatively minor and shallow, having little effect on the frame's performance. In contrast, as shown in Fig. 14, Frame CJ, which contained CJs, exhibited significantly different behavior. At 2% drift, deep and extensive cracks were observed in critical points of the frame. These cracks, resulting from weak concrete bonding in the CJ region, indicated a severe reduction in structural integrity and strength. Specifically, the cracks in this frame rapidly propagated, drastically impacting its seismic performance. As the experiment progressed and displacement increased, at 3% drift, major portions of the beam-to-column connection in Frame CJ failed, with more pronounced damage observed at the joints. The structural weakness was so severe that large sections of concrete were displaced, and the connection's integrity was entirely lost. These observations clearly demonstrate the detrimental effect of CJs on the structure's seismic performance and underscore the necessity of reinforcing such areas. Fig. 15 pertains to Frame RCJ, where, due to the application of FRP sheets at the joints, direct observation of crack depth and length was not possible. The FRP covering obstructed detailed monitoring of surface cracks during testing. However, the hysteresis curves and overall behavior of this frame indicate the positive and significant impact of the FRP sheets at the joints. The FRP sheets effectively enhanced the seismic performance of the structure, particularly by reducing the extent and severity of damage in critical areas and improving the frame's energy absorption and dissipation capacity. In essence, the presence of FRP at the joints prevented premature failure and strengthened the connection region, thereby improving the structure's ductility and stability under cyclic loads.

4.2 Hysteretic of results

Hysteresis loops typically exhibit unique patterns of elastic and plastic deformations and the amount of dissipated energy during cyclic seismic loading. These loops effectively demonstrate the specimens' capacity to absorb and dissipate energy, as well as their stiffness and ductility under repeated loads. As seen in Figs. 16 to 18, the hysteresis plots for the CJ, RJ, and RCJ specimens illustrate how each frame responded differently to the applied loads:

- Frame RJ (no CJs): this frame is a monolithic structure without CJs. Its hysteresis curve indicates favorable behavior, as its capacity did not decrease during the test and it demonstrated good stability. This optimal performance is attributed to the absence of CJs, which enhances the frame's integrity and overall performance.

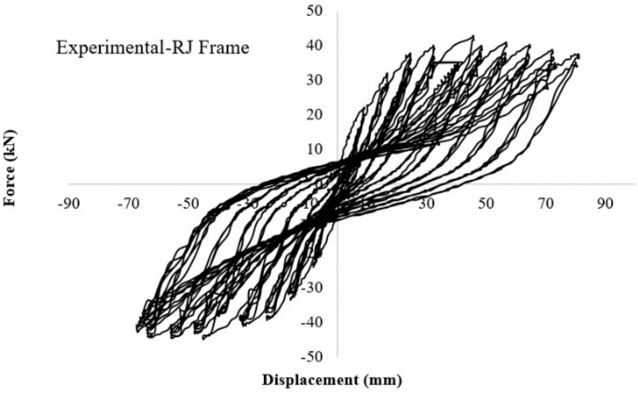

Fig. 16 Hysteresis curve in the RJ frame without CJ

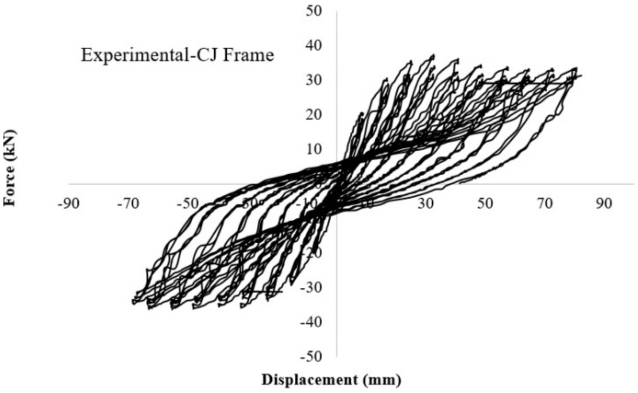

Fig. 17 Hysteresis curve in the CJ frame with CJ

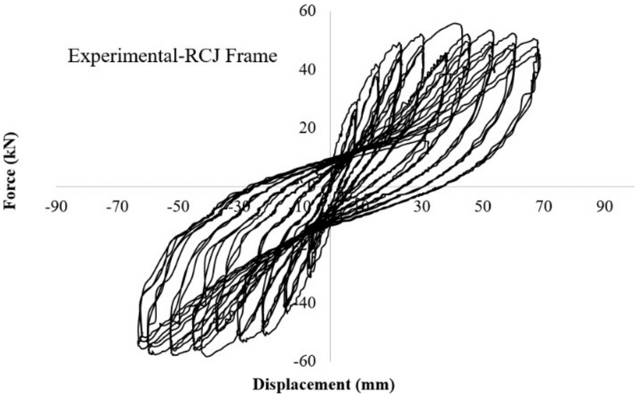

Fig. 18 Hysteresis curve in the FRP-retrofitted RCJ frame

- Frame CJ (with CJs): Frame CJ has CJs and initially exhibited similar behavior to Frame RJ. However, during the test, a significant reduction in resistance was observed, and its hysteresis curve is somewhat slimmer and smaller compared to those of Frames RJ and RCJ. This reduction in resistance and the slimness of the curve are due to the presence of CJs, which have adversely affected the frame's integrity and performance.
- Frame RCJ (reinforced with FRP): Frame RCJ, which is reinforced with FRP sheets, initially showed high resistance and greater initial stiffness compared to the other two frames. However, due to the FRP reinforcement, the frame has become more brittle, with reduced ductility compared to the other frames. Despite this, the energy dissipation in this frame is higher than in the other frames, and its hysteresis curve is broader and larger. This frame demonstrates the highest ultimate resistance, although its ductility is lower due to the brittleness introduced by the FRP reinforcement. Table 7 presents a summary of the results from the hysteresis curves.

4.3 Stiffness degradation

The stiffness degradation is reflected by K_j, and the formula for calculating K_j is shown in Eq. (1):

$$K_j = \frac{\sum_{i=1}^{n} F_{ij}}{\sum_{i=1}^{n} \Delta_{ij}}, \tag{1}$$

where F_{ij} represents the maximum force applied during the i-th cycle under the j-th loading level, and Δ_{ij} represents the top displacement corresponding to F_{ij}. Fig. 19 illustrates the changes in stiffness (K_j) under various displacements. With increasing displacement, especially in the CJ specimen, a significant reduction in stiffness was observed. This decrease is mainly due to concrete cracking and the effects of CJs, which are exacerbated with the progression of loading, particularly at higher displacement ranges. Concrete cracking reduces contact and bonding between structural components, while CJs decrease integrity and increase vulnerabilities in the structure. These issues lead to a significant reduction in stiffness and overall performance of the structure.

4.4 Ductility

The computed values of ductility (μ) for the specimens are presented in Table 7. The parameters of Table 7 are introduced in Fig. 20. The formula for calculating the ductility coefficient (μ) is shown in Eq. (2):

$$\mu = \frac{\Delta_u}{\Delta_y}. \tag{2}$$

As shown in Table 7, among the three frames, Frame RJ exhibits the highest ductility. This frame, being monolithic and free of CJs, demonstrates superior deformation capacity and a greater ability to absorb and dissipate energy during seismic events. The absence of CJs contributes to its enhanced ductility by providing a more uniform response under loading, which leads to better flexibility and adaptability to deformations.

In contrast, Frame RCJ, despite having higher initial stiffness and resistance due to the use of FRP reinforcement, exhibits lower ductility. The FRP reinforcement increases the frame's initial load-bearing capacity and stiffness, improving its performance in terms of resistance to initial deformations. However, this reinforcement also results in increased brittleness. The frame's ability to undergo plastic deformation and absorb energy decreases because FRP, while enhancing stiffness, does not improve ductility.

Instead, it makes the frame stiffer and less flexible, reducing its capacity for sustained deformation under load.

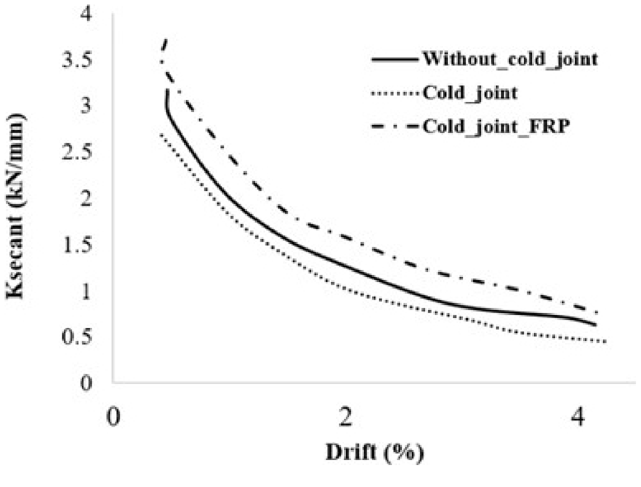

Fig. 19 The degradation characteristics of stiffness for specimens

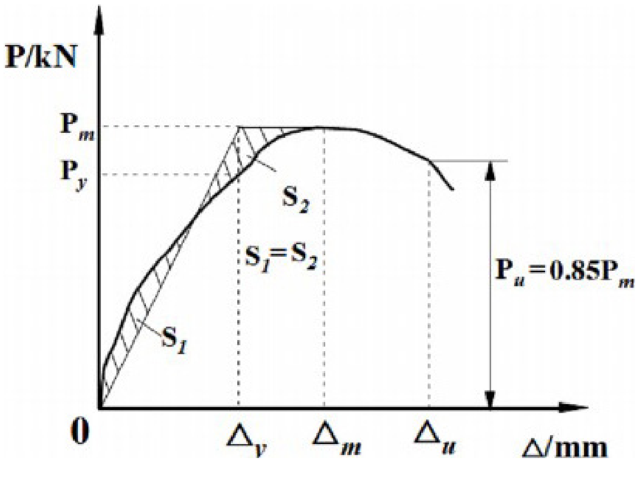

Fig. 20 Evaluation of ductility in frames

Table 7 Comparing the results obtained from the hysteresis curve of experimental specimens

Specimen name	Load direction	Δ_y (mm)	P_y (KN)	Δ_{mm} (mm)	P_m (KN)	Δ_u (mm)	P_u (KN)	μ
RJ specimen	Positive	35.3	29.05	54.9	43.48	69.3	36.95	1.96
	Negative	−34.11	−30.45	−55.80	−40.93	−56.8	−33.58	
CJ specimen	Positive	34.68	26.05	41.33	36.85	55.27	31.32	1.59
	Negative	−29.36	−27.53	−39.50	−34.33	−50.36	−29.18	
RCJ specimen	Positive	44.25	33.86	51.62	56.85	54.23	48.32	1.22
	Negative	−42.36	−32.87	−51.27	−51.37	51.35	−43.66	

This brittleness in Frame RCJ is evident in its hysteresis curve, which, although indicating higher energy dissipation, shows a significant reduction in deformation capacity compared to Frame RJ. The added stiffness provided by FRP does not translate into better ductility but rather results in a stiffer and more brittle response. These changes highlight the limitations of using FRP reinforcement to improve stiffness without addressing the need for plastic deformation and energy dissipation.

4.5 Dissipated energy

A comparison of the gross energy dissipated by specimens can be used to assess their dynamic performance and their capacity to dissipate energy which can be referred to as:

$$E_s = \sum_{i=1}^{n} S_{ABCDA}, \qquad (3)$$

where, "i" refers to the i-th hysteresis cycle, while "S_{ABCDA}" denotes the entire area enclosed by the hysteresis loops.

As illustrated in Fig. 21, the areas enclosed by the force-displacement hysteresis loop can be used to calculate the energy absorbed due to the deformation of the frames. This energy dissipation offers valuable insights into the structural behavior under cyclic loading, emphasizing the frames' capacity to resist and dissipate seismic forces effectively. Such analysis is critical for evaluating the resilience of structures during seismic events and understanding their ability to maintain stability under dynamic loads.

To calculate the cumulative energy dissipation, first, the energy dissipation for each hysteresis cycle must be determined. In each loading cycle, the area enclosed by the hysteresis curve, depicted as a force-displacement diagram, represents the energy dissipated in that cycle, and this area is obtained by integrating the force with respect to displacement. After calculating the energy dissipated in each cycle, these values are summed to determine the cumulative energy absorbed up to that stage of loading. Thus, the cumulative energy dissipation represents the total amount of energy that the structure or specimen has absorbed and dissipated under repetitive (cyclic) loading. Fig. 22 illustrates the cumulative energy dissipation for all three specimens.

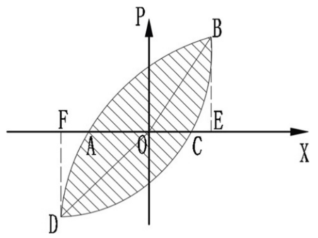

Fig. 21 Determination of energy dissipation

5 Numerical results and discussion

5.1 Hysteresis envelope

Figs. 23 and 24 show the results of the hysteresis envelope obtained from Abaqus and experimental specimens in RJ and CJ specimens.

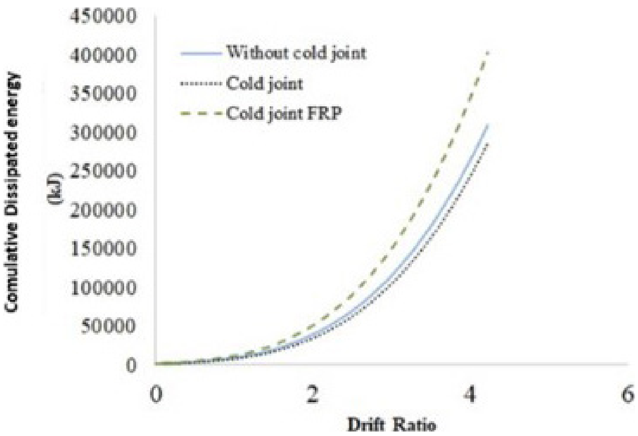

Fig. 22 Comparing the cumulative energy dissipation curve

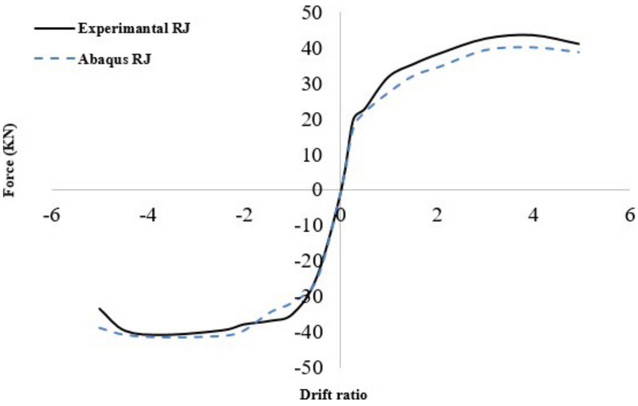

Fig. 23 Comparing the hysteresis envelope curve of the experimental and numerical CJ specimens

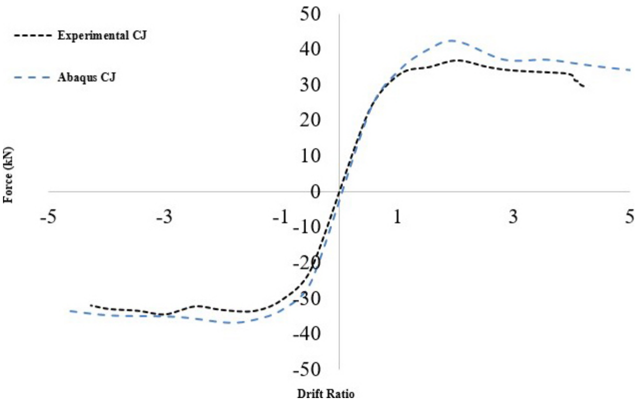

Fig. 24 Comparison of the hysteresis envelope curves between the experimental and numerical RJ specimens

Figs. 23 and 24 illustrate the consistency between the simulation results obtained from Abaqus and the experimental results for both RJ and CJ specimens. The minor differences observed can be attributed to the assumptions made in the numerical models and discrepancies between the numerical models and the experimental specimens. However, since these differences are below 5%, the results are considered acceptable and show good agreement.

5.2 Stress

After confirming that the results of hysteresis curves for both experimental samples and numerical models were closely aligned, and ensuring the accuracy and reliability of the numerical models, we proceeded to the next stage of the investigation. In this stage, we focused on examining and comparing the stresses induced in the structures by analyzing the results obtained from these models. This analysis involved a detailed evaluation of stress values and structural behavior under various loading conditions, which provided us with a deeper understanding of the structural performance and the agreement between numerical models and experimental data. Such comparisons enhanced our ability to assess the precision and predictive capability of numerical models in simulating structural behavior under different loading scenarios, and laid the groundwork for more precise analyses and future optimizations. This phenomenon underscores the importance of thoroughly investigating and analyzing CJ areas. The presence of CJs not only affects stress distribution but also introduces weaknesses and serious issues in structural performance. Therefore, identifying and assessing the impacts of CJs on structural behavior is crucial for the analysis and design of earthquake-resistant structures and other dynamic loading scenarios. The comparison included the assessment of tensile and compressive damage as well as the evaluation of von Mises stresses in the frames. This analysis helped us understand the behavior of structures under different loading conditions and identify the strengths and weaknesses of the numerical models. The results of these analyses are clearly depicted in the contour plots shown in Figs. 25 to 27. Figs. 25 to 27 provide an overview of the distribution of stresses and damages in the frames, allowing for a more accurate assessment of their performance and stability.

As shown in Figs. 25 to 27, the amount of tensile and compressive damage, as well as the stresses present in frames with CJs, is significantly higher compared to other frames. This increase in stress and damage is clearly attributed to the presence of CJs in these structures. Detailed analysis of the stress and damage contours indicates that plastic hinges have formed at the connections of the frames.

5.3 Dissipated energy

In Fig. 28 a comparison of the cumulative energy absorption for the numerical models is also shown. As can be seen, the energy absorbed by the frame without a cold joint is approximately 8% higher than the frame with a CJ. This result is roughly the same as that obtained in the experimental models.

6 Two structural designs to improve the CJ frame behavior

Section 6 proposes two structural designs for improving the behavior of the CJ frame. These designs were

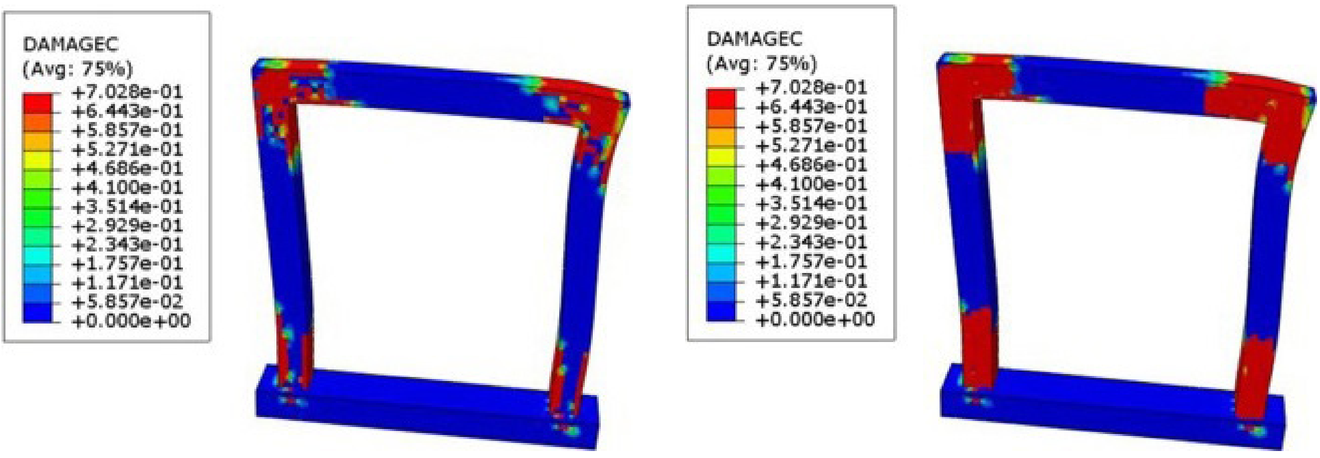

(a) (b)

Fig. 25 Contour of compressive damage in models at the conclusion of the analysis at 5% drift; (a) Control frame; (b) Frame with CJ

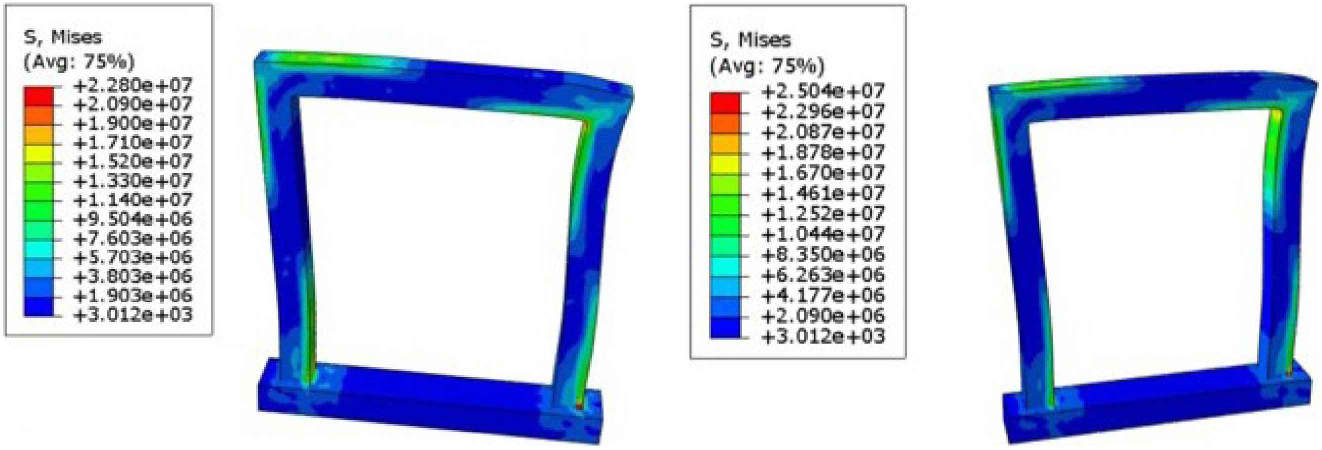

(a) (b)

Fig. 26 Stress distribution in models at the end of analysis at 5% drift; (a) Control frame; (b) Frame with CJ

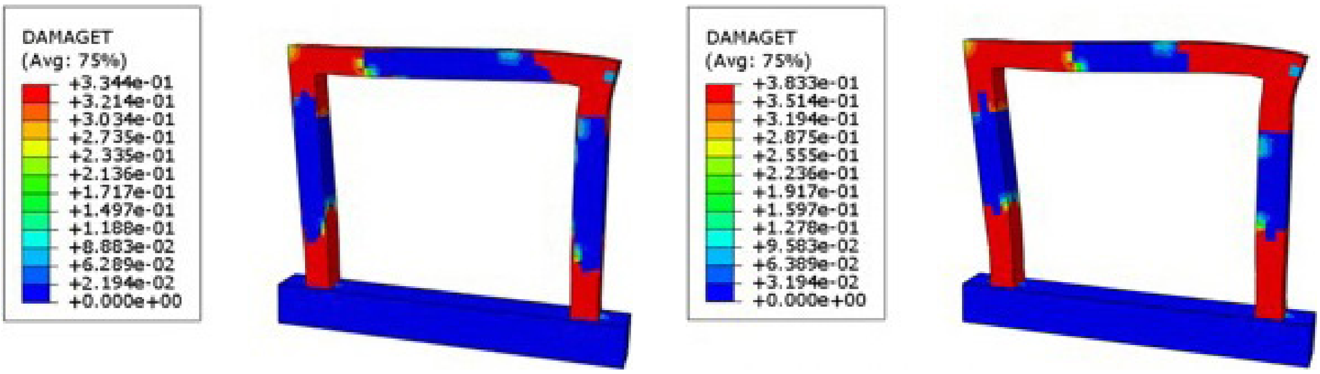

(a) (b)

Fig. 27 Stress distribution in models at the end of analysis at 5% drift; (a) Control frame; (b) Frame with CJ

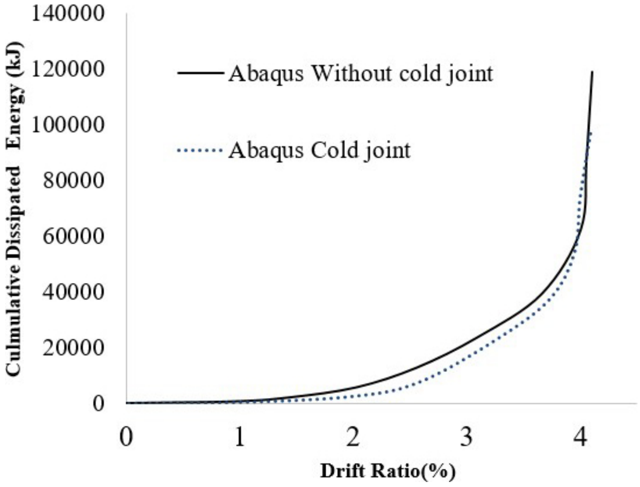

Fig. 28 Comparison of the cumulative energy absorption charts in the numerical models

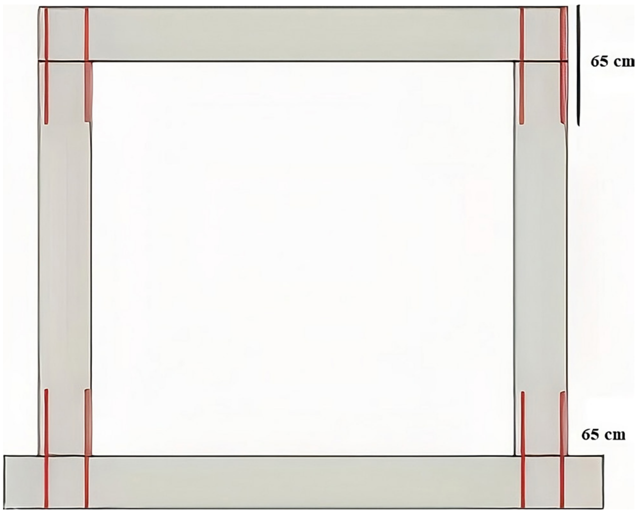

Fig. 29 Frame geometry in the DBCJ structural design

numerically analyzed using Abaqus software. The two proposed designs are:

1. Double bar cold joint (DBCJ): this design includes four tie bars with a 14 mm diameter, as detailed in Fig. 29.
2. Shear key cold joint (SKCJ): This design incorporates a shear key for improved structural performance.

A schematic representation of these two structural designs is shown in Figs. 29 and 30.

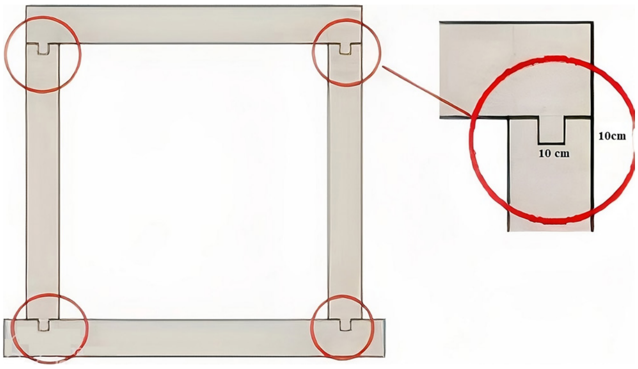

Fig. 30 Frame geometry in the SKCJ structural design

The parameters of the numerical models for these two specimens are consistent with those of the CJ specimen. Section 6.1 discusses the results from both the numerical and experimental models.

6.1 Results of the proposed structural designs versus with RJ and CJ frames

Section 6.1 presents the results for the RJ and CJ numerical models and two enhanced structural designs, which incorporate a shear key and double tie bars. Fig. 31 illustrates the hysteresis envelope curves for these four numerical models, providing a clear comparison of their performance. According to Fig. 31, the CJ frame, which includes CJs, exhibits the lowest lateral load-bearing capacity among the models tested. This reduced capacity highlights the negative impact of CJs on structural performance under seismic conditions. In contrast, the RJ frame, which does not have CJs, demonstrates the highest lateral load-bearing capacity among the analytical models. This superior performance underscores the advantage of avoiding CJs in structural design. Additionally, the frame with the shear key and double tie bars, denoted as SKCJ, showed improved performance compared to the frame with only double tie bars (DBCJ). Despite this improvement, both SKCJ and DBCJ frames still exhibited lower lateral load-bearing capacities compared to the RJ frame. These results indicate that while adding a shear key can enhance performance, it does not fully compensate for the disadvantages associated with CJs. The detailed results of this comparison are summarized in Table 8.

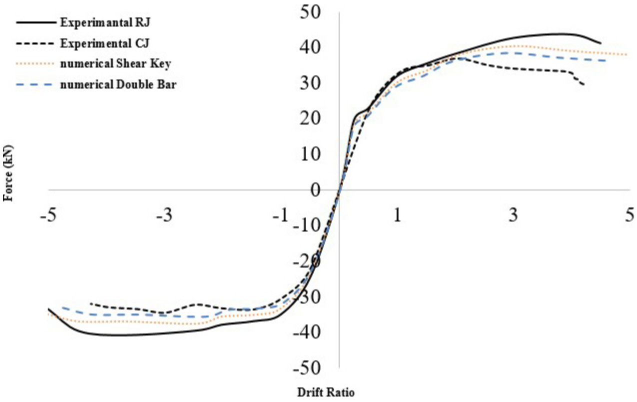

Fig. 31 Compares the hysteresis envelope curves of the four models analyzed in this research

7 Conclusions

This research investigated the behavior of a concrete frame under different conditions, including frames with and without CJs, both experimentally and numerically. Subsequently, these frames were retrofitted using FRP sheets.

Three experimental specimens were prepared: one without a CJ, one with a CJ, and one with an FRP-RCJ. They underwent simultaneous axial and cyclic loading. Additionally, two models – one with a CJ and one without – were simulated using Abaqus software under the same loading regime as the experimental setup. The following results were obtained:

- In specimens with a CJ in the column, the first crack appeared precisely at the CJ. Failure occurred due to hinge formation at the CJ region of the column, followed by a similar failure at the beam. Furthermore, frames without CJs exhibited surface cracks at drifts above 2%, whereas frames with CJs developed surface cracks at drifts of only 1%.
- By introducing a CJ in the structure, the load-carrying capacity in the hysteresis curve decreased by 18% compared to the control frame, indicating a significant reduction in the structure's ability to withstand lateral loads. Additionally, the ductility of the structure, which is a measure of its ability to undergo plastic deformations without failure, decreased by 25%, meaning the structure is less capable of withstanding large deformations after the formation of the CJ. Furthermore, the cumulative dissipated energy, which represents the frame's ability to absorb and dissipate earthquake energy, was reduced

Table 8 Comparison of the results of the hysteresis curve of experimental specimens

Specimen name	Maximum load-bearing capacity (KN)	Increase or decrease compared to the RJ specimen (%)
RJ specimen	43.48	–
CJ specimen	36.85	−17
SKCJ specimen	40.3	−7
DBCJ specimen	38.05	−14

by up to 10%. These reductions clearly demonstrate the negative impact of the CJ on the overall performance of the structure.

- In the frame where the CJ was reinforced with FRP sheets, the lateral load-carrying capacity significantly increased, improving by up to 54%. This increase is due to the reinforcement provided by the FRP, which enhances the structure's resistance to lateral loads. Additionally, the cumulative dissipated energy, indicating the frame's ability to absorb and dissipate seismic energy, rose by up to 33%, demonstrating that the FRP-reinforced frame can better absorb earthquake forces and perform more effectively. However, the use of FRP sheets resulted in a reduction in ductility by up to 30%, as FRP increases stiffness, causing the frame to exhibit more brittle behavior. While the reinforced frame can endure higher loads, its capacity to undergo large deformations before failure is diminished. This reduction in ductility is especially critical in severe earthquakes, as it implies a decreased ability to absorb and dissipate energy from large deformations.
- Two retrofitted structural designs were analyzed using Abaqus: one with double-stitched rebar in the CJ and another with a shear key in the CJ. Results were compared with numerical results from the control frame and the frame with a CJ. The shear key CJ frame exhibited a 6% increase in load-bearing capacity compared to the double-stitched rebar CJ frame.

References

[1] ACI "ACI 318-19(22) Building Code Requirements for Structural Concrete and Commentary (Reapproved 2022)", American Concrete Institute, Indianapolis, IN, USA, 2022.
https://doi.org/10.14359/51716937

[2] Tschegg, E. K., Stanzl, S. E. "Adhesive power measurements of bonds between old and new concrete", Journal of Materials Science, 26(19), pp. 5189–5194, 1991.
https://doi.org/10.1007/BF01143212

[3] Li, G., Xie, H., Xiong, G. "Transition zone studies of new-to-old concrete with different binders", Cement and Concrete Composites, 23(4–5), pp. 381–387, 2001.
https://doi.org/10.1016/S0958-9465(01)00002-6

[4] Lim, Y. M., Kim, M. K., Shin, S. K., Li, V. C. "Numerical Simulation for Quasi-Brittle Interface Fracture in Cementitious Bi-material System", In: de Borst, R., Mazars, J. (eds.) Fracture Mechanics of Concrete Structures, Swets & Zeitlinger, 2001, pp. 73–80. ISBN 90-2651-825-0

[5] Chandra Kishen, J. M., Rao, P. S. "Fracture of cold jointed concrete interfaces", Engineering Fracture Mechanics, 74(1–2), pp. 122–131, 2007.
https://doi.org/10.1016/j.engfracmech.2006.01.017

[6] Roy, B., Laskar, A. I. "Cyclic behavior of in-situ exterior beam-column subassemblies with cold joint in column", Engineering Structures, 132, pp. 822–833, 2017.
https://doi.org/10.1016/j.engstruct.2016.12.001

[7] Roy, B., Laskar, A. I. "Beam–column subassemblies with construction joint in columns above and below the beam", Magazine of Concrete Research, 70(2), pp. 71–83, 2018.
https://doi.org/10.1680/jmacr.17.00155

[8] Bekem Kara, İ. "Experimental Investigation of the Effect of Cold Joint on Strength and Durability of Concrete", Arabian Journal for Science and Engineering, 46(11), pp. 10397–10408, 2021.
https://doi.org/10.1007/s13369-021-05400-5

[9] Qusay Ali, Q., Erdil, B., Mohammed Jassam, T. "Critical cold joint angle in concrete", Construction and Building Materials, 409, 133881, 2023.
https://doi.org/10.1016/j.conbuildmat.2023.133881

[10] Deng, H.-S., Fu, H.-L., Wu, Y.-M., Zhao, Y.-B., Yi, H.-D. "Fatigue fracture experiment of concrete members with cold joints under low stress and low stress amplitude fatigue load", Theoretical and Applied Fracture Mechanics, 127, 104041, 2023.
https://doi.org/10.1016/j.tafmec.2023.104041

[11] Men, B., Qin, Y., Zhang, X., Wu, J., Liang, D., Li, M., Zhou, H. "Investigation on the change of shear strength of concrete with cold joint under the action of sulfate dry–wet cycles", Journal of Building Engineering, 73, 106770, 2023.
https://doi.org/10.1016/j.jobe.2023.106770

[12] Qin, Y., Men, B., Liang, D., Geng, K., Zhang, X., Zhou, H., Liu, R. "Energy evolution of concrete with cold joint under the action of sulfate dry-wet cycles with loading", Journal of Building Engineering, 68, 106098, 2023.
https://doi.org/10.1016/j.jobe.2023.106098

[13] Deng, H.-S., Fu, H.-L., Li, H., Shi, Y., Huang, Z. "Fracture performance and fracture characteristics of concrete members with cold joints: Numerical simulation", Theoretical and Applied Fracture Mechanics, 125, 103868, 2023.
https://doi.org/10.1016/j.tafmec.2023.103868

[14] Deng, H.-S., Fu, H.-L., Chen, W., Zhao, Y.-B., Yi, H.-D. "Study on deterioration, cracking mechanism and treatment measures of plain concrete lining with cold joints in high-speed railroad tunnel", Case Studies in Construction Materials, 18, e01895, 2023.
https://doi.org/10.1016/j.cscm.2023.e01895

[15] Kim, K.-S., Park, K.-T., Jung, K.-S., Kim, R. E., Ali, T., Park, C. "Development of a novel connection method using expanded rib and spiral bars for reinforced concrete beams with cold joints", Engineering Structures, 295, 116863, 2023.
https://doi.org/10.1016/j.engstruct.2023.116863

[16] Fu, H., Deng, H., Zhang, J., Shi, Y., Huang, X. "Experimental Analysis of Influence of Pouring Interval on Fracture Performance of Concrete Structures with Cold Joints", Social Science Research Network, 2021.
https://doi.org/10.2139/ssrn.3977378

[17] Feng, Z., Li, C., Ke, L., Yoo, D.-Y. "Tensile behavior of ultra-high-performance fiber-reinforced concrete (UHPFRC) structure with cold joints", Engineering Structures, 273, 115084, 2022. https://doi.org/10.1016/j.engstruct.2022.115084

[18] Firdaus, M., Saggaff, A., Tahir, M. M., Aghlara, R., Sulaiman, A., Aminuddin, K., Ngain, S. P., Salih, M. N. A. "Influence of seat angles on the behaviour of cold-formed steel concrete composite joints", Journal of Constructional Steel Research, 173, 106246, 2020. https://doi.org/10.1016/j.jcsr.2020.106246

[19] Kurata, M., Nakashima, M., Suita, K. "Effect of Column Base Behaviour on the Seismic Response of Steel Moment Frames", Journal of Earthquake Engineering, 9(sup2), pp. 415–438, 2005. https://doi.org/10.1142/S136324690500247X

[20] ACI "ACI PRC-374.2-13 Guide for Testing Reinforced Concrete Structural Elements under Slowly Applied Simulated Seismic Loads", American Concrete Institute, Indianapolis, IN, USA, 2013.

[21] ABAQUS "Abaqus, (6.14)", [computer program] Available at: http://62.108.178.35:2080/v6.14/index.html

[22] Karimi, E., Kalatjari, V. R. "Numerical Modeling for Simulation of Opening Mode in Fracture Mechanic of Concrete Cold-Joint", Sharif Journal Civil Engineering, 36(2), pp. 61–70, 1979. https://doi.org/10.24200/j30.2019.51286.2388

[23] Lim, Y. "CoMat - Abaqus input file generator for concrete damaged plasticity model", 2024. https://doi.org/10.13140/RG.2.2.25509.10725

[24] Wahalathantri, B. L., Thambiratnam, D. P., Chan, T. H. T., Fawzia, S. "A Material Model for Flexural Crack Simulation in Reinforced Concrete Elements Using ABAQUS", In: Proceedings of the First International Conference on Engineering, Designing and Developing the Built Environment for Sustainable Wellbeing, Brisbane, Australia, 2011, pp. 260–264. ISBN 978-0-9805827-4-1

[25] de Oliveira Ribeiro, P., de Miranda Saleme Gidrão, G., Vareda, L. V., Carrazedo, R., Malite, M. "Numerical and experimental study of concrete I-beam subjected to bending test with cyclic load", Latin American Journal of Solids and Structures, 17(3), e266, 2020. https://doi.org/10.1590/1679-78255880